


Article

# Effect of $YAl_2$ Particles on the Corrosion Behavior of Mg–Li Matrix Composite in NaCl Solution

Zihan Chen <sup>1</sup>, Chonggao Bao <sup>1,\*</sup>, Guoqing Wu <sup>2</sup>, Yongxin Jian <sup>1</sup> and Li Zhang <sup>1</sup>

<sup>1</sup> State Key Laboratory for Mechanical Behavior of Materials, School of Materials Science and Engineering, Xi'an Jiaotong University, Xi'an 710049, Shaanxi Province, China; doyen\_chen@stu.xjtu.edu.cn (Z.C.); yxjian@xjtu.edu.cn (Y.J.); lily3113004001@stu.xjtu.edu.cn (L.Z.)

<sup>2</sup> School of Materials Science and Engineering, Beihang University, Beijing 100191, China; guoqingwu@buaa.edu.cn

\* Correspondence: cgbao@xjtu.edu.cn; Tel.: +86-29-8266-8538

Received: 4 January 2019; Accepted: 10 February 2019; Published: 12 February 2019



**Abstract:** The strength of Mg–Li alloy is greatly improved by the composite strengthening of intermetallic compound  $YAl_2$  particles, but the low corrosion resistance of Mg–Li alloy is still the main factor that restricts the application of the alloy and its composites. In this paper, the effect of  $YAl_2$  particles on the corrosion behavior of Mg–Li alloy was systematically investigated. The results showed that the corrosion resistance of  $YAl_{2p}/LA143$  composite could be significantly improved, accounting for the formation of a transitional interface layer by adding  $YAl_2$  particles. The diffusion of yttrium and aluminum atoms from  $YAl_2$  particulates improved the stability of the surface film and enhanced the adhesion between the corrosion products and the substrate, which hindered further expansion of pitting.

**Keywords:** magnesium; intermetallics; metal matrix composites; XPS; polarization; EIS

## 1. Introduction

Mg–Li-based alloys are currently the lightest among the metallic structural materials, characterized with many excellent properties such as high specific strength, mechanical casting properties, good damping capacity, good thermal conductivity and electromagnetic shielding performance [1,2]. Thus, Mg–Li-based alloys have great potential to be applied in aerospace applications, automobiles, electronic products, etc. [3–6]. However, Mg–Li alloys have the inherent problems of low absolute strength, high chemical activity and poor corrosion resistance, which could decrease their mechanical stability and limit their extensive use [7–10]. It is known that compound reinforcement is a possible way to increase strength and stiffness of Mg–Li-based alloys and prevent mechanical properties degradation.

S.J.Wang and G.Q.Wu et al. [11] developed an Mg–Li matrix composite reinforced with intermetallic compounds (5 wt.%  $YAl_2$  particulates) by stirring casting technique. The  $YAl_2$  particulates uniformly dispersed inside the matrix alloy, and the mechanical properties of the composite were significantly improved. The tensile strength, elastic modulus and hardness of composite were increased by 45.3%, 44.7% and 58.2%, respectively, compared with the initial matrix alloy. In spite of the excellent mechanical properties, poor corrosion resistance has become a critical issue that restricts the applications of Mg–Li composite material. The weak corrosion resistance of Mg–Li-based alloys is mainly caused by the presence of Li, a highly electrochemical and chemically active element. The addition of Li causes a significant increase in the chemical activity of the alloy [12]. Besides, for magnesium-based composites, the addition of the enhanced phase usually exacerbates the corrosion of the matrix [13]. The structural defects caused during composite preparation, such as tiny cracks,

pores, and corrosion galvanic pairs, result in increased localized corrosion of the substrate, hence the magnesium matrix composite material is generally easier to be corroded than the magnesium alloy. In addition, the enhanced phase may destroy the integrity of the protective film on the composite surface, promoting the local corrosion of the composite material. Some magnesium-based composites are severely corroded during manufacture, storage, and transportation [14].

In recent years, several researchers [15–18] have reported that the corrosion behavior and morphology of magnesium alloys are related to alloy composition and environmental conditions. The atmospheric corrosion mechanism of magnesium alloys is mainly caused by the electrochemical destruction of the combined action of oxygen, moisture, and corrosive media contained in the marine atmosphere. When there is a hygroscopic solid depositing on the metal surface, it can absorb water from the atmosphere and promote the formation of a thin liquid film on the metal surface, inducing and aggravating the electrochemical corrosion process. NaCl has strong hygroscopicity as one of the major solid deposits in the marine atmosphere. In addition,  $\text{Cl}^-$  will increase the conductivity of the electrolyte membrane and promote the dissolution of the metal. They have found that pitting corrosion tends to occur on the surface of the magnesium alloys in the presence of  $\text{Cl}^-$ .

Yet, to the best of our knowledge, only few researchers have reported the corrosion performance of Mg–Li alloys [19,20], as well as the systemic investigations of the corrosion behaviors. Furthermore, only few literature is available on the effect of the composite phase on corrosion performance of Mg–Li-based alloys. Therefore, the corrosion behaviors of Mg–Li matrix composite with and without  $\text{YAl}_2$  particles were systematically investigated by immersion test in 3.5 wt.% NaCl solution.

## 2. Materials and Methods

### 2.1. Materials and Solutions

The  $\text{YAl}_2$  reinforced Mg–Li matrix composite was prepared by stirring casting in an electrical resistance furnace under a protective argon atmosphere. The raw materials included 5 wt.%  $\text{YAl}_2$  intermetallic compound (0.5–3  $\mu\text{m}$ ) and the base matrix alloy Mg–14Li–3Al (LA143). Before solidification, the superheated slurry (680  $^\circ\text{C}$ ) was stirred at 700 r.p.m. for 30 min. After casting, the materials were extruded under 300  $^\circ\text{C}$  at a speed of 0.5 mm/s. The density of  $\text{YAl}_{2\text{p}}$ /LA143 composite and LA143 alloy is 1.42  $\text{g}/\text{cm}^3$  and 1.37  $\text{g}/\text{cm}^3$ .

The  $\text{YAl}_2$  reinforced Mg–Li matrix composite is mainly composed of  $\text{YAl}_2$  particles and ( $\beta$ )-Li phase. As shown in Figure 1a,  $\text{YAl}_2$  particles are uniformly dispersed in the matrix. However, the LA143 alloy only contains ( $\beta$ )-Li single-phase, as shown in Figure 1b.

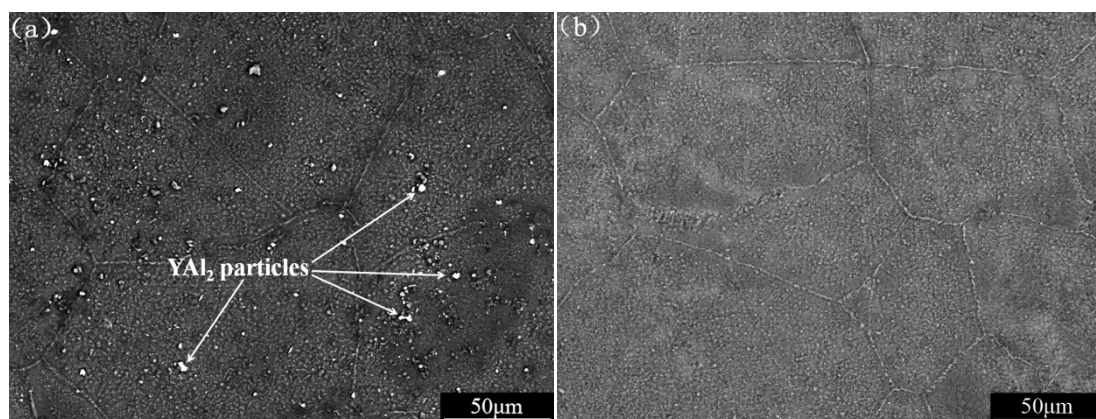


**Figure 1.** The SEM (backscatter electron) micrograph of (a)  $\text{YAl}_2$  reinforced LA143 matrix composite and (b) LA143 alloy.

In the experiment, the  $\text{YAl}_{2\text{p}}$ /LA143 composite and LA143 alloy were cut into individual samples with a size of  $\Phi 16 \text{ mm} \times 3 \text{ mm}$ . Then the samples were orderly ground by 600#, 800#, 1000#, 1500#,

2000# SiC sand paper, and then polished on flannelette with that aiming to  $R_a \leq 1.0 \mu\text{m}$ . During the polishing process, anhydrous ethanol was used to scrub the sample surface. After polishing, the sample was ultrasonically washed in acetone solution for less than 5 min.

In the marine atmosphere, magnesium alloys are vulnerable to corrosion due to the existence of  $\text{Cl}^-$ . To simulate the corrosion medium, 3.5 wt.% NaCl solution was prepared by analytically pure reagents and distilled water during the corrosion performance test.

## 2.2. Immersion Test

Firstly, the standard samples of LA143 alloy and  $\text{YAl}_{2\text{p}}$ /LA143 composite were divided into 6 groups which were then immersed into 3.5 wt.% NaCl solution at the temperature of 298 K. The testing time for each group was respectively set as 12 h, 24 h, 36 h, 48 h, 60 h and 72 h. The ratio of solution volume to specimen surface area ( $2 \text{ cm}^2$ ) was  $20 \text{ mL}/\text{cm}^2$  according to the Chinese national standards (JB/T 7901-1999). After immersion, the corrosion products of each sample were removed by a chromic acid solution composed of  $\text{CrO}_3$  (200 g/L) and  $\text{AgNO}_3$  (10 g/L) according to the Chinese national standards (GB/T 16545-1996). The corrosion rate  $R$  ( $\text{gm}^{-2}\text{h}^{-2}$ ) can be calculated by measuring the sample mass before and after immersion following the Equation (1):

$$R = \frac{M - M_1}{ST} \quad (1)$$

where  $M$  (g) and  $M_1$  (g) are the mass before and after corrosion,  $S$  ( $\text{m}^2$ ) is the area of corroded surface and  $T$  (h) is corrosion duration [21].

Meanwhile, to keep the reproducibility of the result, the same measurement were conducted three times for each group. The final data was derived from the average of the three independent measurements results.

## 2.3. Electrochemical Measurements

The corrosion resistance of LA143 alloy and  $\text{YAl}_{2\text{p}}$ /LA143 composite were analyzed by ELDY/CS-310 electrochemical station (Zhonghui Tiancheng Technology Co., Ltd., Beijing, China). A three-electrode system worked during the electrochemical measurement. A platinum electrode was used as the auxiliary electrode, a saturated calomel electrode (SCE) as the reference electrode, while a standard sample with the exposed surface of  $1 \text{ cm}^2$  as the working electrode.

The detection time of the open circuit potential (OCP) was 1 h. The potentiometric polarization curves were used to study the protective performance of  $\text{YAl}_2$  metal compounds at a scan rate of  $2 \text{ mV}/\text{s}$ . Electrochemical impedance spectroscopy (EIS) was used to analyze the corrosion behavior with scanning frequencies from 10 mHz to 100 kHz. Zsimpwin software (Version 3.10, EChem Software, Ann Arbor, MI, USA) was used to collect, fit, and analyze experimental data.

## 2.4. Microstructure Characterization

The surface morphology after corrosion was observed by a scanning electron microscopy (SEM, VEGAL XMUINCA) (TESCAN, Brno, Czechoslovakia) with energy dispersive analysis of X-ray (EDAX) (Oxford Instruments, Oxford, United Kingdom). In addition, a 3D laser scanning microscope (VK-9710K) (KEYENCE, Osaka, Japan) was used to help analyze the three-dimension morphology of the corrosion surface. Corrosion products were analyzed using the X-ray diffraction (XR, X'PERT PR) (BRUKER, Karlsruhe, Germany) and X-ray photoelectron spectroscopy (XPS) (SHMADZU, Kyoto, Japan).

### 3. Results and Discussion

#### 3.1. Immersion Test

Figure 2a shows the weight loss of LA143 alloy and  $\text{YAl}_{2p}/\text{LA143}$  composite after immersion in 3.5 wt.% NaCl solution as a function of time. It can be seen that the weight loss of the LA143 alloy is nearly two times larger than that of the composite. After 72 h, the weight loss of LA143 alloy rises up to  $944.95 \text{ g/m}^2$  while the  $\text{YAl}_{2p}/\text{LA143}$  composite is  $596.88 \text{ g/m}^2$ . In order to further explore the corrosion process of these two materials, the corrosion rate during the immersion test was calculated according to the results of the corrosion weight loss, as shown in Figure 2b. The corrosion rate of LA143 alloy is higher before 24 h and then declines gradually. However, for  $\text{YAl}_{2p}/\text{LA143}$  composite, the corrosion rate decreases slightly before 24 h and then becomes stable. It is worth noting that the corrosion rate of both materials shows a slightly increase in the last 12 h. By comparison, the  $\text{YAl}_{2p}/\text{LA143}$  composite presents better corrosion resistance behavior.

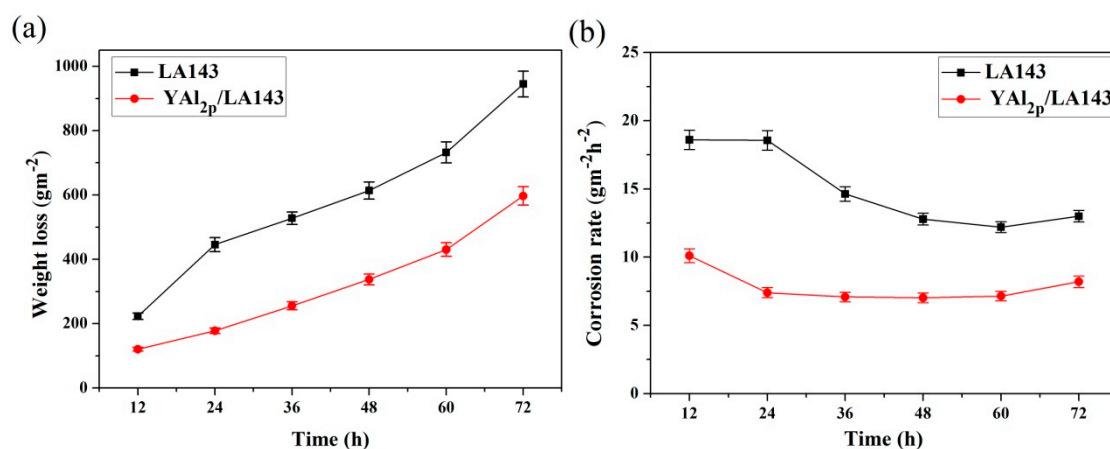


**Figure 2.** Curves of the LA143 alloy and  $\text{YAl}_{2p}/\text{LA143}$  composite corrosion at 298 K for 72 h in 3.5 wt.% NaCl solution. (a) Weight loss versus time and (b) corrosion rate versus time.

The main reason for the poor corrosion resistance of magnesium alloys is that  $\text{Mg}(\text{OH})_2$ , the main component of the surface film, is not stable in acidic, neutral, and weak alkaline solutions [17,22]. In particular, when the solution contains highly corrosive ions, such as  $\text{Cl}^-$  which can transform the protective  $\text{MgO}/\text{Mg}(\text{OH})_2$  into soluble  $\text{MgCl}_2$ , the dissolution of magnesium may be accelerated [23]. At the same time, a large amount of  $\text{H}_2$  is precipitated during the corrosion process, which further reduces the denseness of the surface film.

In the initial stage of corrosion, the corrosion rate is high because the surface film of the LA143 alloy and the  $\text{YAl}_{2p}/\text{LA143}$  composite material are not well protected. When the sample is directly exposed to NaCl solution, it is severely damaged by  $\text{Cl}^-$ . As the duration of corrosion increases, the corrosion products are gradually formed on the surface of the material, which prevent the diffusion of the  $\text{Cl}^-$  to the substrate. In addition, the presence of the corrosion product layer hinders the efficient transport of charge, resulting in a decrease of corrosion rate.

From the above results, we conclude that the addition of  $\text{YAl}_2$  particulates plays a significant role in inhibiting the corrosion solution, and thus, improves the corrosion resistance of the composites to a certain degree. However, the mechanism of action should be comprehensively analyzed.

In order to explore the mechanism of  $\text{YAl}_2$  particles on the surface film and corrosion resistance of Mg–Li alloy, the surface corrosion morphologies of LA143 alloys and  $\text{YAl}_{2p}/\text{LA143}$  composites after 72 h immersion were observed and analyzed. Before we removed the corrosion products from the sample surface, we observed that the corrosion products on the composite were more cohesive than those on the LA143 alloy. The specific difference between the two samples after 72 h immersed was that the corrosion products on LA143 alloys gradually fell off as the corrosion proceeded. On the

contrary, the most corrosion products on the  $YAl_{2p}/LA143$  composite were adhered to the surface of the sample, but it was too loose to protect the matrix from  $Cl^-$  erosion and could be removed easily.

Figure 3 shows the surface corrosion morphologies of LA143 alloys and  $YAl_{2p}/LA143$  composites after 72 h immersion in 3.5 wt.% NaCl solution after removing the corrosion products. It can be seen that the corrosion surface of the LA143 alloys (Figure 3a) is flatter than the  $YAl_{2p}/LA143$  composites (Figure 3b), indicating the uniformity corrosion of the LA143 alloy. On the contrary, the corroded surface of the composite is very rough, with a large number of crater-shaped protrusions and numerous corrosion pits. Furthermore, the three-dimensional morphologies of the corrosion surface were detected by 3D laser scanning microscopy, as shown in Figure 4. Compared with the LA143 alloy, several protrusions can be obviously observed on the corrosion surface of the  $YAl_{2p}/LA143$  composites, which is consistent with the SEM observations. These protrusions are supposed to be the  $YAl_2$  particles. In this case, the protruded  $YAl_2$  particles may change the corrosion mode and hinder the further expansion of the pitting, which benefits to improvement of the corrosion resistance.

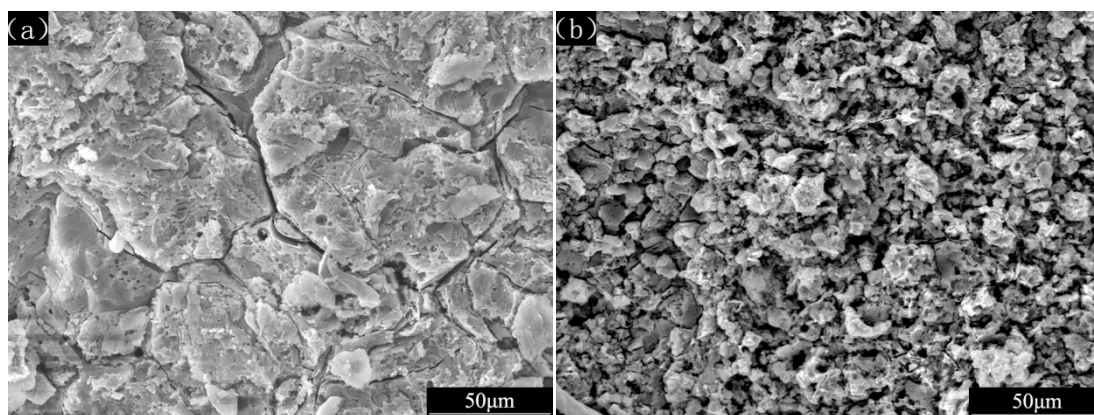


**Figure 3.** The SEM (secondary electron) micrograph of (a) LA143 alloys and (b)  $YAl_{2p}/LA143$  composites' surface after 72 h immersion in 3.5 wt.% NaCl solution.

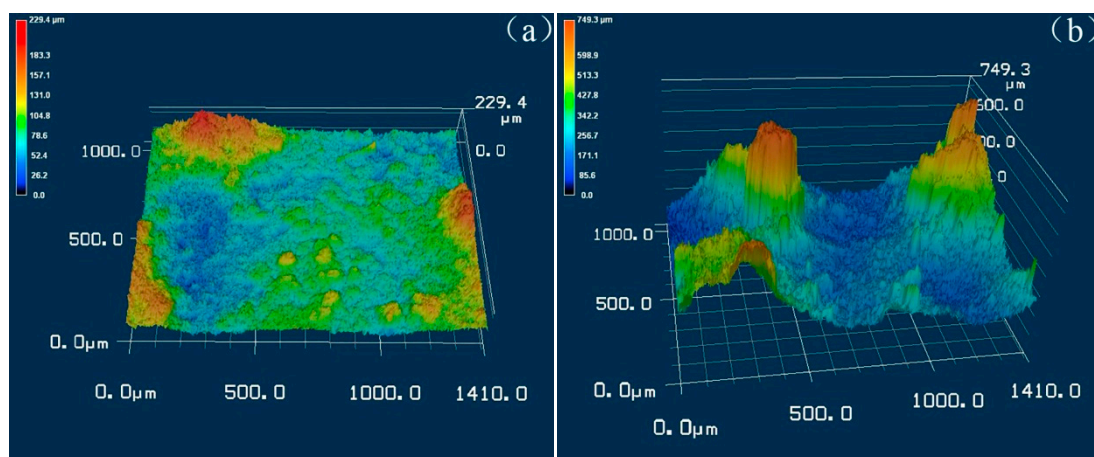


**Figure 4.** The 3D laser scan image of (a) LA143 alloys and (b)  $YAl_{2p}/LA143$  composites' surface after 72 h immersion in 3.5 wt.% NaCl solution.

In order to clarify the formation of the characterized corrosion surface of the  $YAl_{2p}/LA143$  composite, the chemical composition of the protrusion was determined by EDS (Energy Dispersive Spectrometer), as shown in Figure 5. In this figure, three spots were detected on the top of the protrusions. Spot 1 is exactly on the  $YAl_2$  particle, while spot 2 and spot 3 are gradually away from the  $YAl_2$  particle on the base alloy. The detecting results of the chemical compositions are shown in Table 1. The weight percentages of Al (15.76%) and Y (28.16%) are relatively high, as the detecting point is on

the  $YAl_2$  particle. It is worth noting that Al (7.24% and 7.44%) and Y (7.96% and 7.43%) could also be detected on spots 2 and 3. In this context, it can be concluded that Al and Y could diffuse into the surrounding substrate. In the previous study [24], due to the agglomeration problem within the matrix caused by the size reduction of the reinforcement particles during the composite preparation, the  $YAl_2$  particles were surface-modified with a compound ball mill method. During ball milling, the surface of  $YAl_2$  particles was covered by Mg film. With the extension of ball milling time and the continuous loading of mechanical force, atomic diffusion occurred between  $YAl_2$  and Mg, forming a metallurgical bonding interface. Therefore, in the composite material prepared by adding this  $YAl_2$ /Mg composite powder to the matrix alloy, there exists a transitional interface layer with a certain width between the reinforcement and the base body, which is dominated by the diffusion of yttrium and aluminum atoms.

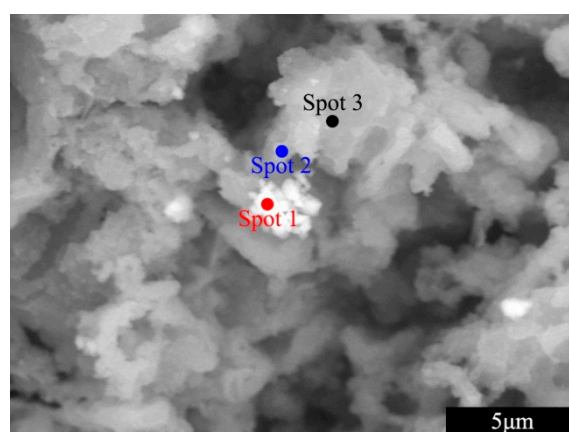


**Figure 5.** The EDS image (backscatter electron) of  $YAl_{2p}$ /LA143 composites' surface after 72 h immersion in 3.5 wt.% NaCl solution.

**Table 1.** The weight percentage of element for spot scanning in Figure 5.

Element	Weight Percentage (wt.%)		
	Spot 1	Spot 2	Spot 3
C	0.70	0.60	0.72
O	7.25	5.02	5.10
Mg	16.70	30.99	44.85
Al	15.76	7.24	7.44
Cl	0	1.34	0.87
Cr	31.43	46.85	33.58
Y	28.16	7.96	7.43

Several researchers found that the addition of Al and Y into certain commercial alloys (AZ91) or binary Mg alloys (Mg–Y, Mg–Al) had a positive effect on the corrosion resistance [25–27]. On the one hand, in the neutral environment, Al can form  $Al_2O_3$  phase to protect the matrix on the surface of magnesium alloy. Additionally, Al addition can also improve the stability of the  $Mg(OH)_2$  film, benefiting to the improvement of the corrosion resistance. On the other hand, Y has the same standard electrochemical potential ( $-2.372$  V SHE (Standard Hydrogen Electrode)) as Mg, which can tremendously improve the corrosion resistance of the magnesium alloy [27]. Luo et al. [25] reported that the corrosion resistance of AZ91 alloy could be improved with Y addition less than the critical content of 0.3 wt.%. Therefore, the diffusion of Y and Al is supposed to improve the corrosion resistance of the  $YAl_{2p}$ /LA143 composite.

In order to investigate the effect of diffused Y and Al on the surface film of the  $YAl_{2p}$ /LA143 composite, the corrosion products of the alloy and the composite were analyzed by XRD and XPS. The XRD spectrum of the corrosion products are shown in Figure 6 that the corrosion products of both alloy and composite are  $Mg(OH)_2$  and LiOH. In addition, an incomplete corrosion phase of

$\text{Li}_{0.92}\text{Mg}_{0.48}$  is detected, the appearance of which can reflect the corrosion has been suppressed to a certain extent. Compared with the LA143 alloy, the corrosion products of  $\text{YAl}_{2\text{p}}/\text{LA143}$  composite contains higher content of  $\text{Li}_{0.92}\text{Mg}_{0.48}$ , indicating the composite exhibits a higher degree of corrosion inhibition. The XPS analysis suggests that the compositions of the immersion product film on the surface of both LA143 alloy and  $\text{YAl}_{2\text{p}}/\text{LA143}$  composite are mainly composed of  $\text{Mg}(\text{OH})_2$ ,  $\text{LiOH}$ ,  $\text{MgCO}_3$ ,  $\text{Li}_2\text{CO}_3$  and a small amount of  $\text{Al}_2\text{O}_3$ , as shown in Figure 7. However,  $\text{Y}_2\text{O}_3$  (Figure 7a) can be found in  $\text{YAl}_{2\text{p}}/\text{LA143}$  composite which is formed by the diffusion of Y from  $\text{YAl}_2$  particles. According to the reports of Luo et al. [25],  $\text{Y}_2\text{O}_3$  can help to improve the stability of the surface film. From Figure 7b,c, it is shown that the diffusion of Y promotes the transition from Al to  $\text{Al}_2\text{O}_3$ , which improves the relative density of the surface film. As shown in Figure 7d–g, a significant increase of  $\text{Li}_2\text{CO}_3$  is observed according to the peaks of C 1s and Li 1s, which agrees well with the results of Eriksson et al. [28]. On the other hand, Xu et al. [29] found, Mg and Li would oxidize preferentially to produce  $\text{MgO}$  and  $\text{Li}_2\text{O}$  when the Mg–Li alloy was exposed to atmospheric air. Subsequently,  $\text{Li}_2\text{O}$  reacted with atmospheric  $\text{CO}_2$  to generate the  $\text{Li}_2\text{CO}_3$  layer. Due to the existence of Y,  $\text{Li}_2\text{O}$  can actively react with  $\text{CO}_2$  to generate more  $\text{Li}_2\text{CO}_3$ . The possible reaction process is as the following Equations (2) and (3):

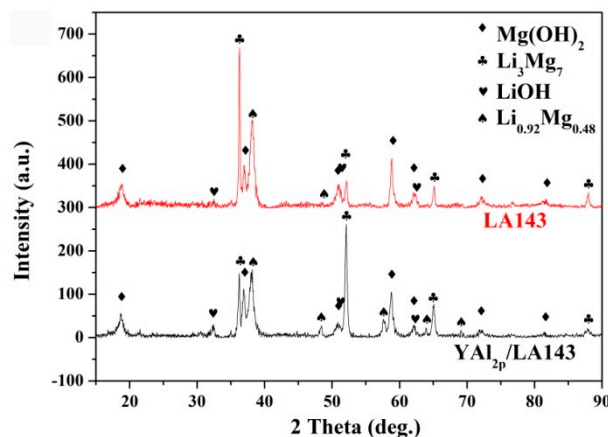


**Figure 6.** XRD analysis of LA143 Alloy and  $\text{YAl}_{2\text{p}}/\text{LA143}$  composite, after immersion test in 3.5 wt.% NaCl solution.

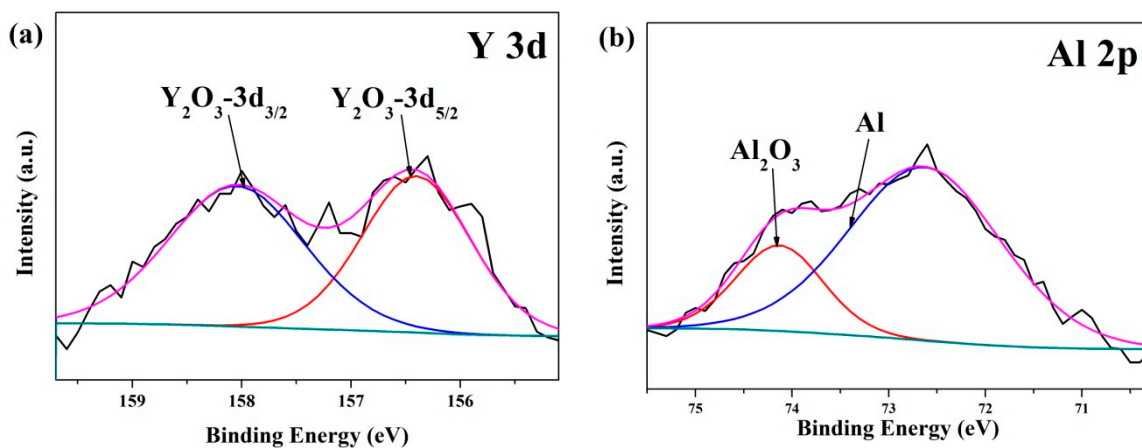


**Figure 7.** Cont.

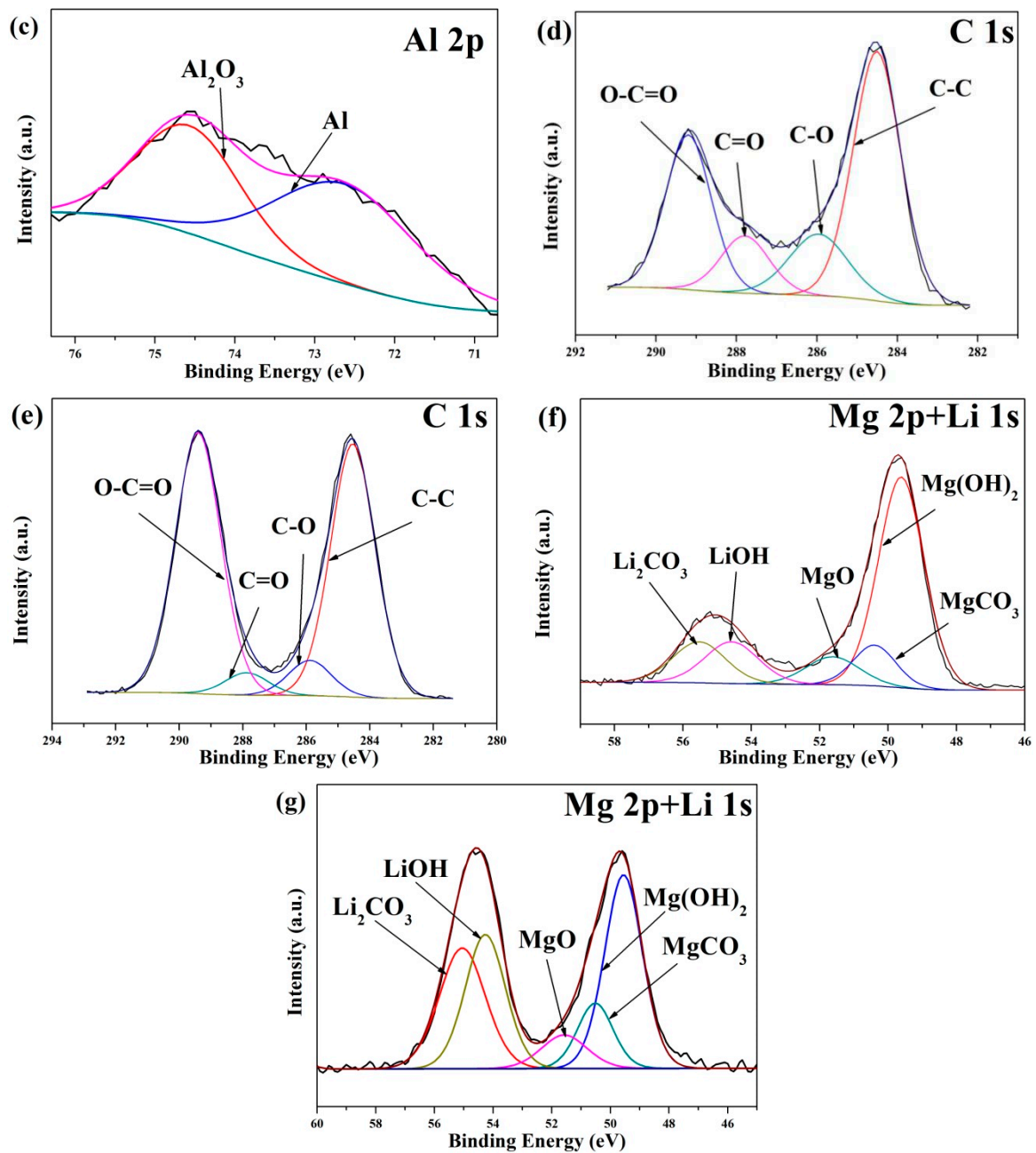


**Figure 7.** XPS analysis of (b,d,f) LA143 Alloy, and (a,c,e,g) YAl<sub>2p</sub>/LA143 composite, after immersion test in 3.5 wt.% NaCl solution.

The presence of Li<sub>2</sub>CO<sub>3</sub> is greatly beneficial to the matrix alloy because of its indissolubility in water and limits the dissolution of the alloy. In Figure 6f and g, the peak of LiOH in YAl<sub>2p</sub>/LA143 composite is obviously higher than that in LA143 alloy. Since LiOH tends to dissolve into the solution, the Li<sub>2</sub>CO<sub>3</sub> layer in the product film can help hinder the dissolution process of LiOH. In YAl<sub>2p</sub>/LA143 composite, the product film is relatively denser, resulting in the better protective effect.

### 3.2. Open Circuit Potential and Potentiodynamic Polarization Measurements

The curves of open circuit potential versus time of YAl<sub>2p</sub>/LA143 composite and LA143 alloy in 3.5 wt.% NaCl solution for 1 h are shown in Figure 8a. As we can see, the OCP of the composite is around  $-1.578$  V, and the OCP of LA143 alloy is about  $-1.623$  V. Although OCP is not related to the corrosion rate, it is still able to reflect the formation process and chemical stability of the oxidation film



on the sample. For LA143 alloy, the OCP declines slowly at the beginning and then becomes stable. However, the change in the OCP of the composite, contrary to that of the alloy, experiences a slow rising at the beginning before its stabilization thereafter. Finally, the potential difference between the alloy and composite is about 0.05 V. This demonstrates that during the corrosion process, the film formed on the surface of the composite is more protective than the alloy. From another perspective, when the composite coupled to other materials, it has a lower galvanic corrosion tendency.

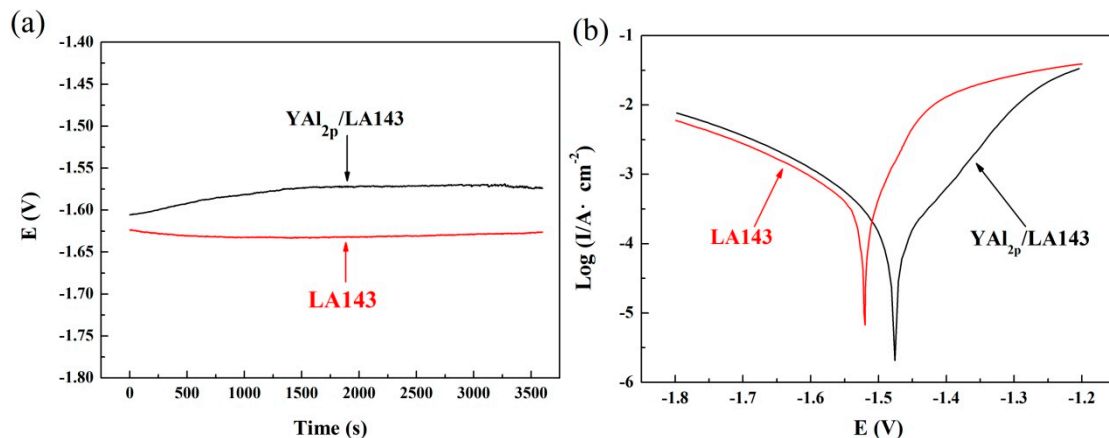


**Figure 8.** The curves of (a) open circuit potential vs time and (b) polarization of YAl<sub>2p</sub>/LA143 composite and LA143 alloy in 3.5 wt.% NaCl solution.

The polarization curves of YAl<sub>2p</sub>/LA143 composite and LA143 alloy in 3.5 wt.% NaCl solution are shown in Figure 8b. The cathodic polarization curves represent the cathode hydrogen evolution through water reduction, whereas the anodic polarization curves show the active dissolving of Mg–Li alloy. As shown in Figure 8b, the YAl<sub>2</sub> particles have little effects on cathodic polarization process. But, the anodic part of YAl<sub>2p</sub>/LA143 composite is characterized by a slowly increase of current density with increasing potentials. However, for LA143 alloy, the current density increases sharply once exceeding the corrosion potential. The lower dissolution rate of YAl<sub>2p</sub>/LA143 composite reveals that a compact and protective corrosion product film is formed on the surface of YAl<sub>2p</sub>/LA143 composite, which is consistent with the results of XPS analysis (Figure 7). In addition, the corrosion potential of YAl<sub>2p</sub>/LA143 (−1.476V) composite is more positive than that of LA143 alloy (−1.521 V).

Generally, the Magnesium alloys often behave as ideal non-polarizable electrodes. Moreover, the anodic branch is strongly affected by the well-known negative difference effect. Therefore, the anodic “Tafel” slope does not correspond to the activation of the charge transfer process. In this case, the corrosion current density was determined only for the estimation of the cathodic currents using the well measured cathodic branch. The corrosion current density ( $I_{\text{corr}}$ ) of YAl<sub>2p</sub>/LA143 composite and LA143 alloy is  $6.6674 \times 10^{-4}$  and  $8.6097 \times 10^{-4}$ . Despite their corrosion current density are in the same order of magnitude, the composite still shows a better corrosion resistance.

### 3.3. EIS Characteristics

Figure 9 presents the Nyquist plots of YAl<sub>2p</sub>/LA143 composite and LA143 alloy in 3.5 wt.% NaCl solution. The plot of each sample consists of two capacitive loops. The high-medium frequency capacitive loop is probably attributed to the mass transport resistance of surface film, while the low frequency capacitive loop is related to the electric double layer capacitance and charge transfer resistance [30]. EIS equivalent circuit is proposed to model the sample/solution interface of YAl<sub>2p</sub>/LA143 composite and LA143 alloy in 3.5 wt.% NaCl solution as shown in Figure 10. The values of equivalent circuit component are summarized in Table 2 after fitting process.

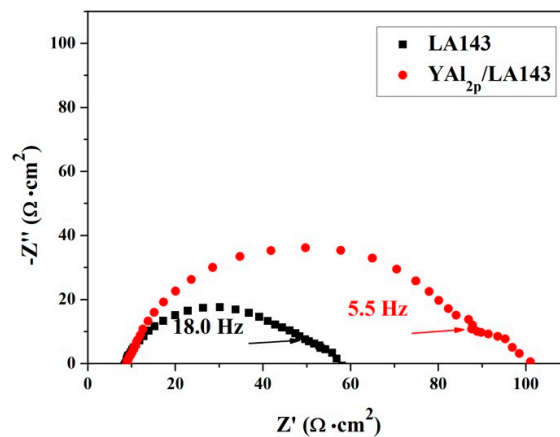


Figure 9. Nyquist plots of LA143 and YAl<sub>2p</sub>/LA143 in 3.5% NaCl solution.

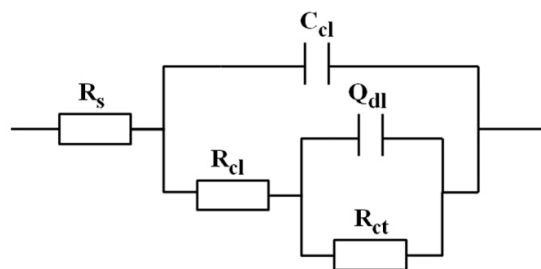


Figure 10. Electrical equivalent circuit diagrams to fit the impedance spectra of LA143 and YAl<sub>2p</sub>/LA143 in 3.5% NaCl solution in Figure 9.  $R_s$ : solution resistance;  $C_{cl}$ : corrosion layer capacitance;  $R_{cl}$ : corrosion layer resistance;  $Q_{dl}$ : double-layer capacitance,  $R_{ct}$ : charge transfer resistance.

As we can see, the capacitive loop of composite is twice as big as that of the alloy. In general, a large capacitive loop means good corrosion resistance and a low corrosion rate. Besides, the value of  $R_{cl}$  and  $R_{ct}$  in the equivalent circuit of LA143 alloy is lower than that of the composite, while the value of  $C_{cl}$  and  $Q_{dl}$  is higher. The value of  $C_{cl}$  can represent the density of corrosion layer. The value is big when the layer is loose textured [31–37]. It is concluded that the addition of YAl<sub>2</sub> particles improves the density of corrosion product. The resistance of corrosion product increases, while the capacitance decreases, which means the YAl<sub>2p</sub>/LA143 composite has a better corrosion resistant property.

Table 2. The parameters of the equivalent circuit of LA143 and YAl<sub>2p</sub>/LA143 in 3.5 wt.% NaCl solution.

Samples	$R_{cl}/\Omega \cdot \text{cm}^{-2}$	$C_{cl}/\text{F} \cdot \text{cm}^{-2}$	$R_{ct}/\Omega \cdot \text{cm}^{-2}$	$Q_{dl}/\text{F} \cdot \text{cm}^{-2}$
LA143 alloy	$27.59 \pm 0.01$	$(4.139 \pm 0.001) \times 10^{-5}$	$13.56 \pm 0.01$	$(2.083 \pm 0.008) \times 10^{-4}$
YAl <sub>2p</sub> /LA143 composite	$61.35 \pm 0.02$	$(2.445 \pm 0.001) \times 10^{-5}$	$17.02 \pm 0.02$	$(1.350 \pm 0.01) \times 10^{-4}$

As above immersion test and electrochemical test results mentioned, the addition of YAl<sub>2</sub> particles not only greatly improves the mechanical properties of the composite material, but also suppresses the corrosion tendency of the matrix. Meanwhile, the diffusion of Y and Al from YAl<sub>2</sub> particles improves the corrosion resistance of YAl<sub>2p</sub>/LA143 composite.

#### 4. Conclusions

The corrosion weight loss of the YAl<sub>2p</sub>/LA143 composite after being immersed in 3.5 wt.% NaCl solution for 72 h is only 63% of that of the LA143 alloy, and the corrosion rate of composite is always kept at a low level. The corrosion surface of the LA143 alloys is uniform, but the corrosion surface of the YAl<sub>2p</sub>/LA143 composites is very rough and possesses a large number of protrusions, and there are numerous corrosion pits. The existence of YAl<sub>2</sub> contributes to the formation of a compact film on the

surface of the substrate and enhances the adhesion between the corrosion products and the substrate by forming  $Y_2O_3$ . Furthermore,  $Al_2O_3$  and  $Li_2CO_3$  in the product film can be also increased, which hinders further expansion of pitting, improving the corrosion resistance of the composite material.

The addition of  $YAl_2$  particles makes the open circuit potential and the corrosion potential of the composite shift positively by 0.05 V, respectively. The anodic polarization curves and Nyquist plots both reveal that a compact and protective corrosion product film is formed on the surface of  $YAl_{2p}/LA143$  composite. As a result, it improves the corrosion resistance.

**Author Contributions:** Conceptualization, Z.C., G.W. and L.Z.; Methodology, Z.C., C.B. and Y.J.; Software, Z.C. and L.Z.; Validation, Z.C., Y.J. and L.Z.; Formal Analysis, Z.C.; Investigation, Z.C. and L.Z.; Resources, G.W.; Data Curation, Z.C.; Writing-Original Draft Preparation, Z.C.; Writing-Review & Editing, C.B., G.W. and Y.J.; Visualization, Z.C.; Supervision, G.W.; Project Administration, C.B.; Funding Acquisition, C.B.

**Funding:** This research was funded by the Research and Development Plan of Shaanxi Province, China (Grant No. 2017GY-118); Science and Technology Innovation Project (Grant No. 009-031-001); and State Key Laboratory for Mechanical Behavior of Materials (Grant No. 20151712).

**Acknowledgments:** I acknowledge Huiqing Fan and Yuchun Chen who helped us to improve the readability of this test. I would further appreciate Qiong Wang who helped us for the experimental works.

**Conflicts of Interest:** The authors declare no conflict of interest.

## References

1. Lin, Y.-N.; Wu, H.-Y.; Zhou, G.-Z.; Chiu, C.-H.; Lee, S. Mechanical and anisotropic behaviors of Mg–Li–Zn alloy thin sheets. *Mater. Des.* **2008**, *29*, 2061–2065. [[CrossRef](#)]
2. Song, G.S.; Staiger, M.; Kral, M. Some new characteristics of the strengthening phase in  $\beta$ -phase magnesium–lithium alloys containing aluminum and beryllium. *Mater. Sci. Eng. A* **2004**, *371*, 371–376. [[CrossRef](#)]
3. Zou, Y.; Zhang, L.; Li, Y.; Wang, H.; Liu, J.; Liaw, P.K.; Bei, H.; Zhang, Z. Improvement of mechanical behaviors of a superlight Mg–Li base alloy by duplex phases and fine precipitates. *J. Alloys Compd.* **2018**, *735*, 2625–2633. [[CrossRef](#)]
4. Zeng, R.-C.; Sun, L.; Zheng, Y.-F.; Cui, H.-Z.; Han, E.-H. Corrosion and characterisation of dual phase Mg–Li–Ca alloy in Hank’s solution: The influence of microstructural features. *Corros. Sci.* **2014**, *79*, 69–82. [[CrossRef](#)]
5. Wu, R.-Z.; Yan, Y.-D.; Wang, G.-X.; Murr, L.E.; Han, W.; Zhang, Z.-W.; Zhang, M.-I. Recent progress in magnesium–lithium alloys. *Int. Mater. Rev.* **2015**, *60*, 65–100. [[CrossRef](#)]
6. Pan, F.; Yang, M.; Chen, X. Technology, A review on casting magnesium alloys: modification of commercial alloys and development of new alloys. *J. Mater. Sci. Technol.* **2016**, *32*, 1211–1221. [[CrossRef](#)]
7. Zhang, H.; Yao, G.; Wang, S.; Liu, Y.; Luo, H.; Technology, C. A chrome-free conversion coating for magnesium–lithium alloy by a phosphate–permanganate solution. *Surf. Coat. Technol.* **2008**, *202*, 1825–1830. [[CrossRef](#)]
8. Song, G.; StJohn, D. Corrosion behaviour of magnesium in ethylene glycol. *Corros. Sci.* **2004**, *46*, 1381–1399. [[CrossRef](#)]
9. Ballerini, G.; Bardi, U.; Bignucolo, R.; Ceraolo, G. About some corrosion mechanisms of AZ91D magnesium alloy. *Corros. Sci.* **2005**, *47*, 2173–2184. [[CrossRef](#)]
10. Yamasaki, M.; Hayashi, N.; Izumi, S.; Kawamura, Y. Corrosion behavior of rapidly solidified Mg–Zn–rare earth element alloys in NaCl solution. *Corros. Sci.* **2007**, *49*, 255–262. [[CrossRef](#)]
11. Wang, S.; Wu, G.; Li, R.; Luo, G.; Huang, Z. Microstructures and mechanical properties of 5 wt.%  $Al_2Yp/Mg-Li$  composite. *Mater. Lett.* **2006**, *60*, 1863–1865. [[CrossRef](#)]
12. Tiwari, S.; Balasubramaniam, R.; Gupta, M. Corrosion behavior of SiC reinforced magnesium composites. *Corros. Sci.* **2007**, *49*, 711–725. [[CrossRef](#)]
13. Pardo, A.; Merino, S.; Merino, M.C.; Barroso, I.; Mohedano, M.; Arrabal, R.; Viejo, F. Corrosion behaviour of silicon–carbide-particle reinforced AZ92 magnesium alloy. *Corros. Sci.* **2009**, *51*, 841–849. [[CrossRef](#)]
14. Hihara, L.H.; Latanision, R.M. Corrosion of metal matrix composites. *Metall. Rev.* **1994**, *39*, 245–264. [[CrossRef](#)]
15. Shi, Z.; Song, G.; Atrens, A. The corrosion performance of anodised magnesium alloys. *Corros. Sci.* **2006**, *48*, 3531–3546. [[CrossRef](#)]

16. Heakal, F.E.-T.; Fekry, A.; Jibril, M.A.E.-B. Electrochemical behaviour of the Mg alloy AZ91D in borate solutions. *Corros. Sci.* **2011**, *53*, 1174–1185. [[CrossRef](#)]
17. Verdier, S.; Van Der Laak, N.; Delalande, S.; Metson, J.; Dalard, F. The surface reactivity of a magnesium–aluminium alloy in acidic fluoride solutions studied by electrochemical techniques and XPS. *Appl. Surf. Sci.* **2004**, *235*, 513–524. [[CrossRef](#)]
18. Hiromoto, S.; Shishido, T.; Yamamoto, A.; Maruyama, N.; Somekawa, H.; Mukai, T. Precipitation control of calcium phosphate on pure magnesium by anodization. *Corros. Sci.* **2008**, *50*, 2906–2913. [[CrossRef](#)]
19. Zhang, C.; Huang, X.; Zhang, M.; Gao, L.; Wu, R. Electrochemical characterization of the corrosion of a Mg–Li alloy. *Mater. Lett.* **2008**, *62*, 2177–2180. [[CrossRef](#)]
20. Xiang, Q.; Jiang, B.; Zhang, Y.; Chen, X.; Song, J.; Xu, J.; Fang, L.; Pan, F. Effect of rolling-induced microstructure on corrosion behaviour of an as-extruded Mg-5Li-1Al alloy sheet. *Corros. Sci.* **2017**, *119*, 14–22. [[CrossRef](#)]
21. Wang, X.; Gao, Y.; Li, Y.; Yang, T. Effect of yttrium on the corrosion behavior of 09CrCuSb alloy in NaCl solution. *Corros. Sci.* **2014**, *87*, 211–217. [[CrossRef](#)]
22. Jönsson, M.; Dan, P.; Thierry, D. Corrosion product formation during NaCl induced atmospheric corrosion of magnesium alloy AZ91D. *Corros. Sci.* **2007**, *49*, 1540–1558. [[CrossRef](#)]
23. Xin, Y.; Huo, K.; Hu, T.; Tang, G.; Chu, P.K. Influence of aggressive ions on the degradation behavior of biomedical magnesium alloy in physiological environment. *Corros. Sci.* **2008**, *4*, 2008–2015. [[CrossRef](#)] [[PubMed](#)]
24. Zhang, Q.; Wu, G.; Huang, Z.; Tao, Y. Compounds, Effects of particle/matrix interfaces on the mechanical properties for SiCp or YAl<sub>2</sub>p reinforced Mg–Li composites. *J. Alloys Compd.* **2014**, *588*, 1–6. [[CrossRef](#)]
25. Luo, T.; Yang, Y.J.M. Design, Corrosion properties and corrosion evolution of as-cast AZ91 alloy with rare earth yttrium. *Mater. Des.* **2011**, *32*, 5043–5048. [[CrossRef](#)]
26. Nouri, M.; Sun, X.; Li, D. Beneficial effects of yttrium on the performance of Mg–3% Al alloy during wear, corrosion and corrosive wear. *Tribol. Int.* **2013**, *67*, 154–163. [[CrossRef](#)]
27. Zhang, X.; Zhang, K.; Deng, X.; Hongwei, L.; Yongjun, L.; Minglong, M.; Ning, L.; Wang, Y. Corrosion behavior of Mg–Y alloy in NaCl aqueous solution. *Prog. Nat. Sci. Mater. Int.* **2012**, *22*, 169–174. [[CrossRef](#)]
28. Eriksson, T.; Andersson, A.M.; Bishop, A.G.; Gejke, C.; Gustafsson, T.; Thomas, J. Surface Analysis of LiMn<sub>2</sub>O<sub>4</sub> Electrodes in Carbonate-Based Electrolytes. *J. Electrochem. Soc.* **2002**, *149*, A69–A78. [[CrossRef](#)]
29. Xu, W.; Birbilis, N.; Sha, G.; Wang, Y.; Daniels, J.E.; Xiao, Y.; Ferry, M. A high-specific-strength and corrosion-resistant magnesium alloy. *Nat. Mater.* **2015**, *14*, 1229–1235. [[CrossRef](#)]
30. Mansfeld, F.; Kendig, M.; Tsai, S. Evaluation of corrosion behavior of coated metals with AC impedance measurements. *Corrosion* **1982**, *38*, 478–485. [[CrossRef](#)]
31. Wang, X.; Gao, Y.; Li, K.; Yan, J.; Li, Y.; Feng, J. Effect of yttrium on the corrosion behaviour of 09CrCuSb alloy in concentrated sulphuric acid. *Corros. Sci.* **2013**, *69*, 369–375. [[CrossRef](#)]
32. Solmaz, R.; Kardaş, G.; Culha, M.; Yazıcı, B.; Erbil, M. Investigation of adsorption and inhibitive effect of 2-mercaptothiazoline on corrosion of mild steel in hydrochloric acid media. *Electrochim. Acta* **2008**, *53*, 5941–5952. [[CrossRef](#)]
33. Özcan, M.; Dehri, I.; Erbil, M. Organic sulphur-containing compounds as corrosion inhibitors for mild steel in acidic media: correlation between inhibition efficiency and chemical structure. *Appl. Surf. Sci.* **2004**, *236*, 155–164. [[CrossRef](#)]
34. Özcan, M.; Karadağ, F.; Dehri, I.J.C.; Physicochemical, S.A.; Aspects, E. Investigation of adsorption characteristics of methionine at mild steel/sulfuric acid interface: an experimental and theoretical study. *Colloids Surf. A Physicochem. Eng. Asp.* **2008**, *316*, 55–61. [[CrossRef](#)]
35. Oguzie, E.; Li, Y.; Wang, F. Corrosion inhibition and adsorption behavior of methionine on mild steel in sulfuric acid and synergistic effect of iodide ion. *J. Colloid Interface Sci.* **2007**, *310*, 90–98. [[CrossRef](#)] [[PubMed](#)]
36. Behpour, M.; Ghoreishi, S.; Soltani, N.; Salavati-Niasari, M. The inhibitive effect of some bis-N, S-bidentate Schiff bases on corrosion behaviour of 304 stainless steel in hydrochloric acid solution. *Corros. Sci.* **2009**, *51*, 1073–1082. [[CrossRef](#)]
37. Umoren, S.; Li, Y.; Wang, F. Synergistic effect of iodide ion and polyacrylic acid on corrosion inhibition of iron in H<sub>2</sub>SO<sub>4</sub> investigated by electrochemical techniques. *Corros. Sci.* **2010**, *52*, 2422–2429. [[CrossRef](#)]

